Desert Ecosystem Engineering Journal

Journal homepage: http://deej.kashanu.ac.ir

University of Kashan

Depositional pattern of sediments in a dry-lake Playa in NE Iran; Implication for geomorphologic characteristics

Maliheh Pourali[1], Adel Sepehr[2]*, Mohamad Hosein Mahmudy Gharaie[3]

Abstract

The depositional pattern of dry lake playa sediments in NE Iran was studied to characterize the surface morphology of the playa based on sediment mineralogy. About 12 topo-soil samples were excavated by hand auger. All topo-soils were collected in three landforms of firm-puffy ground, clay-carbonate crusts, and halite dominated saltpans, to be examined for mineralogy by XRD analysis and physicochemical properties in the lab. XRF analysis performed to define the major oxides of the sediments. Quartz and calcite were the main minerals over the playa. Also, halite and gypsum were the major minerals categorized in the sediments indicating the dominant evaporate process in the area. Based on the results, a high concentration of EC (>48 dS/m) was observed in the mid-southern and southern part of the playa. Besides, the high concentrations of CCE (>27 %) and pH (>9) were observed in the eastern and the western playa, verifying the primary detection of the playa's three major geomorphologic landforms in the fieldwork. A recent depositional pattern of carbonates and chloride formed from eastern to the western parts of the playa, respectively. Nevertheless, central playa shows the areas with the main minerals of calcite and halite. The existence of evaporate minerals depends on a cycle of the wet and dried lake during the Holocene.

Keywords: Evaporate Sediments, Mineral Composition, Geomorphology, Sabzevar Playa.

1. PhD Candidate, Department of Geography, Ferdowsi University of Mashhad, Mashhad, Iran;
2. Associate Professor, Department of Desert and Arid Zones Management, Ferdowsi University of Mashhad. Mashhad. Iran, adelsepehr@um.ac.ir
3. Associate Professor, Department of Geology Faculty of Sciences Ferdowsi University Of Mashhad (FUM). Mashhad. Iran

1. Introduction

In the Quaternary period, the climate conditions have changed globally (Roy et al. 2006) and due to these changes in circulation and variation of climate a worldwide expansion of the deserts have been occurred (Dawson 1992). The sediment records and geomorphologic evidence such as fossilized sand dunes, alluvial fans, palaeo-lakes, and playa dry-lakes are used to detect the climatic change of Quaternary (Thomas 1997). The playas basins located in the desert margins are sensitive to this climatic change (Roy et al. 2006). Such playa lakes in arid regions provide sensitive databases for the paleo-environment studies and climatic changes models in the Quaternary (Street-Perrott and Harrison 1985, Harrison 1993, May et al. 2015). Geomorphologic knowledge of the arid and semi-arid regions has greatly improved in recent years. For instance, the sedimentology, topography, and geomorphology of shoreline, fluvial and aeolian sediments have been used to investigate dry playa lakes in the arid center of Australia by a broad of authors (DeVogel et al. 2004, Magee et al. 2004, Leon and Cohen 2012, Cohen et al. 2015, May et al. 2015). However, the geomorphologic exploration of dry lake playas' sedimentary data has not been studied extensively due to its multidisciplinary nature.

Dry lake playas identified as landforms in arid regions (Abrahams and Parsons 1994). In these landforms, gypsum and salts have the main character in depositional records (Canton et al. 2003). Briere (2000) has proposed a precise definition for playa systems as the intra-continental arid zone basins with annual dryness for over 75% of the time. However, Glennie (1978) has defined playa as a temporary lake in the center of a basin of inland drainage where salts are concentrated by evaporation. He has stated that not all playas supplied by surface water as many of

them have an important or unique groundwater supply (Arche 2008). The first study regarding playas of Iran backs to Krinsley (1970) who distinguished about 60 playas approximately and presented a systematic classification of Kavir surfaces (A Persian term tantamount Sabkha and salt pans). In this article, the spatial dynamics of sediment compositions have been studied along an arid dry-lake playa across Sabzevar in northeastern Iran, where is a small part of the central playa of Iran. The mineral compositions can represent the evidence of regional responses to climate fluctuations during the Quaternary period.

Although many studies have investigated sedimentary depositions worldwide, much of the focus has been on aeolian initiation or palaeo-climate implications (e.g., Thomas and Burrough 2013, Leighton et al., 2014, Li and Yang, 2015, Lancaster et al., 2016, Yang et al. 2018, Vaezi et al. 2019, Gholami et al. 2019). However, the main aim of this study is to investigate the mineralogy and geochemistry of Sabzevar Playa sediments by consuming quantitative and descriptive data as well as spatial and statistical analyzes and the geomorphic changes of the playa in the late Holocene. The importance of this study can be assumed as its role on increase our environmental knowledge about the nature and factors of climate change in the long term because the playa sediments are the best cases to serve the history of past environmental conditions in semi-arid regions.

2. Materials and methods

2.1. General characteristics of the study area

According to the classification of Handford (1981), relating dominant geomorphologic processes in arid regions, Sabzevar dry lake categorized as a typical playa of central playa of Iran called Dasht-Kavir (Kearey 2009). On this basis, Sabzevar playa, which is located in the eastern great Kavir basin, was chosen as the study area with a total surface area of

about 2648 Km² between latitude 35°55'00"- 36°25'00" N and longitude 56°15'00"- 57°45'00" E (Fig. 1a).
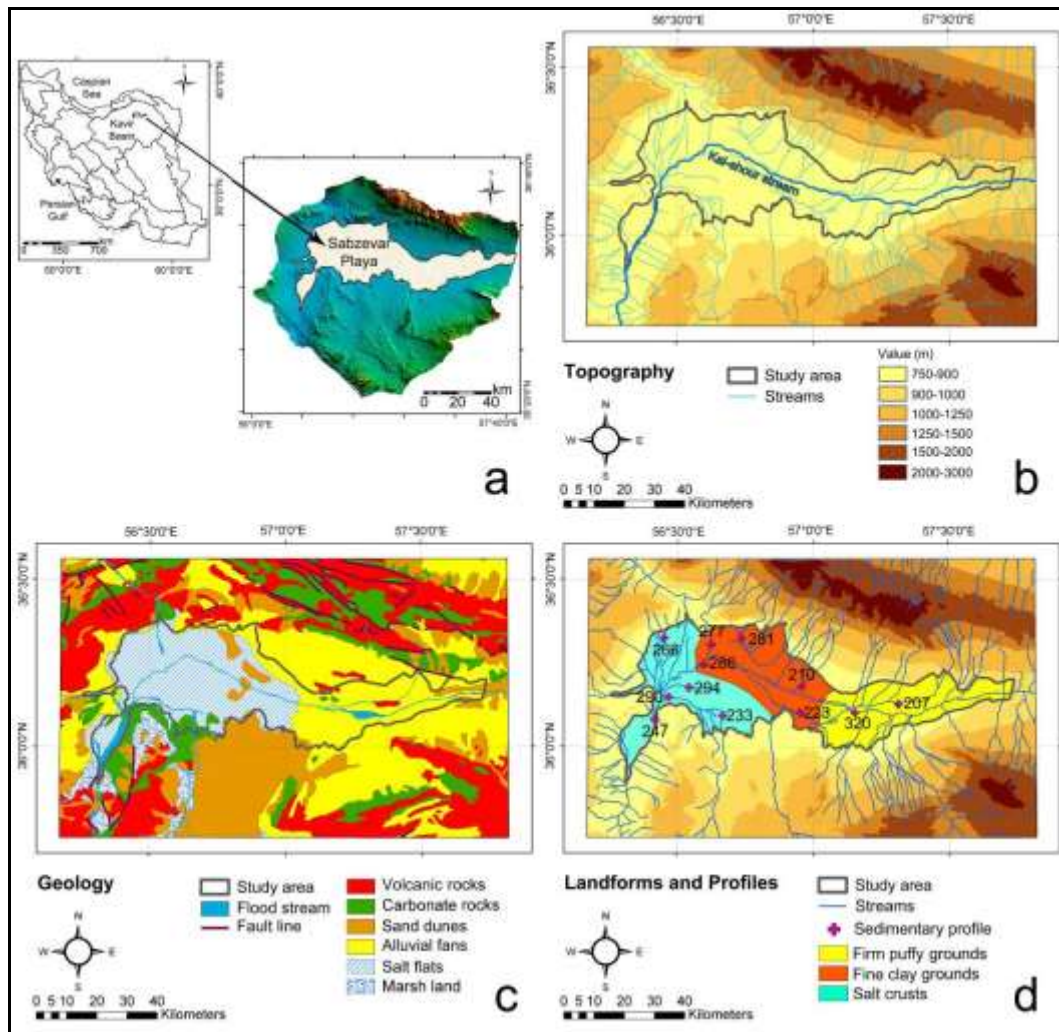
Figure (1): a. General position of the study area in great Kavir basin, central Iran, b. Topographical characteristics, c. Geological map, and d. General position of landforms and location of topo-soils

The topographical elevation values of the study area vary between 750 and 900 m above sea level (m a.s.l), while the main topographical elevation is over 800 m a.s.l over a flat relief. The general topographic trend of the playa extends in the east to west along the Kal-Shour River with an average of 120 Km length (Fig. 1b). Sabzevar playa is a hydrological closed drainage basin with the dried surface. According to Gansser (1955), there was a place of the possible lake, which probably has been closed during the early-Pleistocene epoch. Geologically, the depositional nature of the playa has been developed along with two dominated environments of alluvial sediments and evaporation sediments of salt flats belong to the Quaternary period (Geological Survey of Iran, 2005) (Fig. 1c), which have confirmed the evidence of a dried lake. The end part of the playa formed a salt-marsh land. In addition to wind-borne sand dunes, the volcanic tuffs and pelagic carbonate rocks can be found around the playa, which belongs to the upper Cretaceous period and earlier. The climate of the region is semi-arid with annual precipitation of 150-200 mm and an annual temperature of 16-17 °C (Hijmans et al. 2005). Based on a set of fieldwork observations during the dry season of 2016 (July and

August) about twelve samples were considered in three landforms of firm-puffy ground, clay-carbonate plain with physical crusts, and saltpans with the dominance of halite salts. The general position of three major geomorphologic landforms and location of profiles are presented in Fig. 1d and the general vision of the aforementioned landforms are showed in Fig. 2. In similar research, Farpoor et al. (2012), have identified different geomorphologic surfaces on Sirjan playa, including clay flats, puffy ground, and salt crusts.

The initial geomorphology of the study area was visually investigated using satellite imagery data by ETM+ (color composite: 4-3-2; 5-3-1; 1-5-7), Google Earth™, and fieldwork observations. The geological investigation was studied based on four sheets 7262 (Abbas-Abad), 7362 (Davarzan), 7462 (Bashtin), and 7562 (Sabzevar) at the 1:100,000 scale (Geological Survey of Iran 2005). Based on a set of digital elevation model data scaled at ~10 m pixel size, which have been prepared by official products of Geological Survey of Iran (GSI 2016), topographical elevation data were carried out in ArcGIS (10.2).
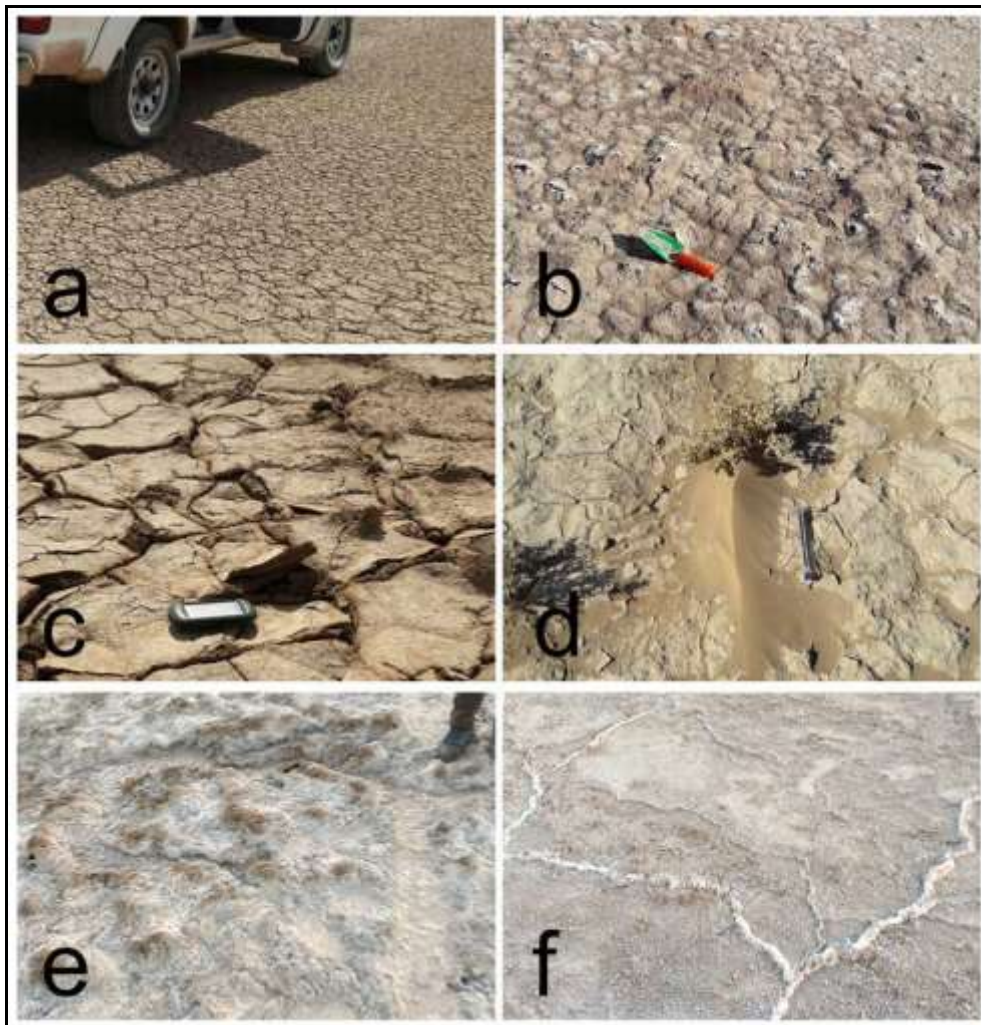
Figure (2): General vision of landforms consisted of firm-puffy ground (e, b), fine-clay ground and embryo Nebka (d), physical carbonate crust (a, c), and salt crusts, Takir (f)

Fieldwork operations were conducted during the dry season of 2016 (July-August), due to proper climatic conditions without any rainfall or runoff phenomena, and were complemented using topographic measurements. In fieldwork, a handheld GPS

was used for general geomorphologic investigation. GPS coordinates and altitudes for each sample location collected in datasets. Then, sampling topo-soils were documented at twelve locations on different surfaces. All topo-soil samples were excavated by hand auger to a depth of ~1 m. The number of samples at each location (topo-soil) was considered through surface and deep profiles, which surface profile was defined from surface to 10-cm depth and other deep profiles were obtained from 10 to 100 cm in depth.

2.2. Analytical methods

All topo-soil samples were measured in the field concerning particle size distribution, and chemical precipitates by the proposed method of May et al. (2015). On this basis, all samples were taken from representative landforms for further analysis in the laboratory of Natural Resources and Environment College. Sediment grain sizes were described using the terminology of Wentworth (1922) and Folk (1954, 1980). To detect sediment grain-size analysis samples were dried and sieved with a set of 0.5 Φ screens in the laboratory after the proposed method of Moussavi-Harami et al. (2004). Based on analyzed data, sediments were classified according to the US Department of Agriculture (USDA) classification scheme. The mineral composition of topo-soil samples was determined by X-ray diffraction (XRD) by PHILIPS PW1730 after Sinha (2006). Powered bulk samples were dried at 50 °C, and XRD charts were generated for the 2θ range of 3-60 °C. Minerals were identified from their characteristic peaks and their relative abundance was estimated from XRD charts. In this regard, evaporite minerals were identified from their characteristic peaks and their relative abundance was estimated from XRD charts. Oriented samples were prepared for fraction of sediments for clay mineralogy using Eppendorf pipette and XRD charts and results

were analyzed by High-score Plus-program to detect the most abundant peaks (Vaezi et al. 2019). The geochemical composition was determined separately for sediments characteristic regarding electrical conductivity (EC), and pH through various analytical techniques at the laboratory of Natural Resources and Environment College of Ferdowsi University of Mashhad. The amount of calcium carbonate equivalent (CCE) was measured by acid neutralization calculated using the SHIBLER method (US Salinity Laboratory Staff 1954). Air-dried sediment samples were heated for 2 h at 420 °C. Besides, X-ray Fluorescence (XRF) was used by PHILIPS PW1410 to analyze major element oxides and trace element concentrations after the standard analytical procedures of Kramar (1997). Meanwhile, the GIS interpolation functions used for analyzing spatial data and visualizing the results (Bagherzadeh and Mansouri Daneshvar 2014). Hence, interpolating the topo-soil dataset was used by geostatistical extension of inverse distance weighting (IDW) to preparing spatial evaluation maps. The geostatistical interpolation algorithms such as the IDW, spline, and Kriging techniques are typical representative methods (Di Piazza et al. 2011, Nikolopoulos et al. 2015). The IDW technique provides a weighting of information that is locally associated and allows the regression model to vary in space. This can help reveal spatial variations in the empirical relationships between factors (Wang et al. 2005, Razmi et al. 2017). In this study, the IDW technique was used to model spatial variation of the geochemical variables both in the surface and depth of the profiles, revealing the less amount of root mean squared and mean predictive errors. The interpolated maps were finally categorized into three classes of negligible, low, and high concentration based on an equal interval method in GIS.

3. Result and Discussion
3.1. Physical and chemical analysis

The location of topo-soils presented in Figure 1d. All physical-chemical properties of EC, pH, CCE, and soil graining analysis are shown in Table 1 for the aforementioned topo-soil samples.

No.	Sample ID	EC (dS/m^{-1})	pH	CCE (%)	Sand (%)	Silt (%)	Clay (%)
				Table (1): Physical-chemical properties of topo-soil samples			
1	207	0.21	7.92	30	78.8	13.2	8
2	210	4.06	8.45	20	88.2	7.3	4.5
3	223	71.34	7.64	24	90.1	8.4	1.5
4	233	8.85	8.18	28	92.3	5.7	2
5	247	37.24	9.39	14	98.1	1.1	0.8
6	266	9.13	9.21	33	91.1	5.5	3.4
7	277	14.14	8.42	28	95.3	2.9	1.8
8	281	30.77	8.17	22	79.6	16.3	4.1
9	286	18.40	9.43	29	75.8	14.6	9.6
10	290	33.66	9.13	21	95.4	1.6	3
11	294	23.47	9.25	32	92.7	6.7	0.6
12	320	26.81	8.11	26	97.8	1.9	0.3

EC: Electrical Conductivity
CCE: Calcium Carbonate Equivalent

Based on Figure 1d, the location of topo-soil 207 in the eastern part of the playa with an elevation of 875 m a.s.l shows a geomorphologic surface categorized as firm puffy ground. The puffy ground also formed by evaporation deposits and therefore evaporate minerals cannot form (Rahimpour-Bonab and Abdi 2012). Dominant geological formation in this landform has been made by Quaternary alluvial fans. According to table 1, EC, pH, and CCE contents in topo-soil 207 were estimated equal 0.21 dS/m, 7.92, and 30 %, respectively. Hence, the surface of this topo-soil is alkaline with the lowest value of electro-conductivity in the study area.

The location of topo-soil 286 (as an indicator auger in clay ground) is in the central part of the playa, in the elevation of 850 m a.s.l., where the geomorphologic surface is categorized as fine clay ground. Polygonal structures are the most common sedimentary features of clay ground. Weak infiltration of these areas could result in to form of mud cracks (Cooke and Warren 1973). Based on the geological map of the study area, terrace deposits and salt flat are dominant geological formations in this landform with physical crusts on the surface. According to Table 1, EC, pH, and CCE contents in topo-soil 286 were estimated equal to 18.40 dS/m, 9.23, and 29 %, respectively. Hence, the surface of this topo-soil is semi-saline with the mid-value of electro-conductivity in the study area.

As well as, the western part of the playa with salt crust surfaces was determined by the location of topo-soil 290 (as an indicator auger in a salt crust) with an elevation of 825 m a.s.l. The geomorphologic surfaces are covered by salt crusts and evaporate depositions, which occurred in the salt flat of lakes and Sabkhas (Watson 1983), dominantly during the end stages of the evaporation era (Rosen 1994). Superficial evaporation causes an upward groundwater association with capillary forces, forming to salt crusts (Rahimpour-Bonab and Abdi 2012). The salt flat is the dominant

geological formation in this landform. EC, pH, and CCE contents in topo-soil 290 were estimated equal 33.66 dS/m, 9.13, and 21 %, respectively (Table 1). Hence, the surface of this topo-soil is saline with a high value of

electro-conductivity in the study area.

In the next step, some interpolation maps were produced for spatial evaluation of EC, pH, and CCE concentrations (Figs. 3a-3c).
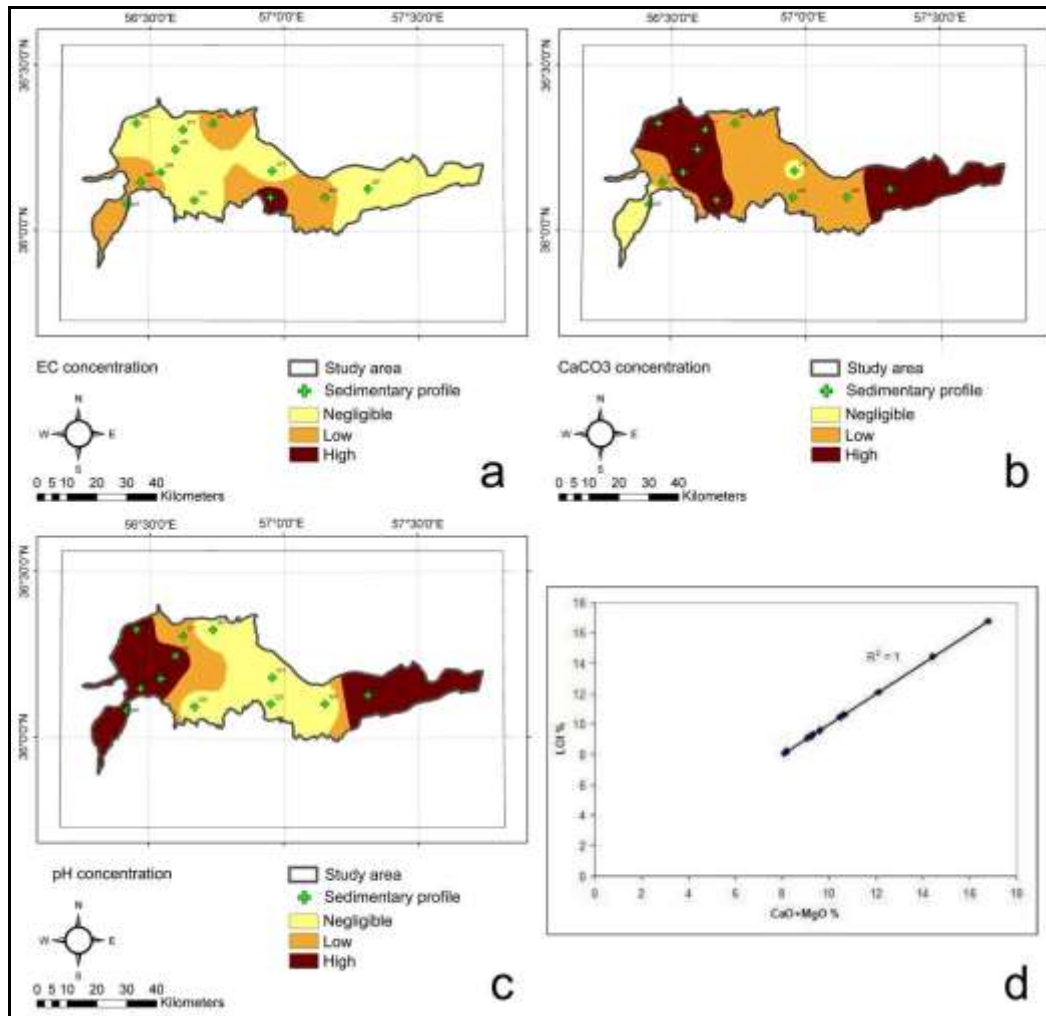
Figure (3): a. Geo-statistical distribution of EC content, b. Geo-statistical distribution of CaCO₃ content, c. Geo-statistical distribution of pH content, and d. Relationship between (CaO+MgO) and L.o.I. in Sabzevar playa

On this basis, a high concentration of EC (>48 dS/m) is observed in the mid-southern and southern part of the playa for instance around the topo-soil samples 223 and 247. Also, the negligible concentration of EC (<24 dS/m) is observed in eastern and western playa around topo-soils 207 and 294. According to Figure 3b, a high concentration of CCE (>27 %) is observed in eastern and western playa around topo-soils 207 and 294. Also, the negligible concentration of CCE (<21 %) is observed in the central and southern part of the

playa for instance around the topo-soils 210 and 247. According to Figure 3c, a high concentration of pH (>9) is observed in western playa around topo-soils 294. Also, the negligible concentration of pH (<8.5) is observed in the central part of the playa for instance around the topo-soils 210 and 223. The aforementioned consequence, which gained from the physical-chemical properties of topo-soil samples, is corresponded to detect of playa's three major geomorphologic landforms in fieldwork observation.

3.2. Geochemical and mineralogical analysis

Based on the results of XRF analysis about 12 major elements and 16 trace elements of selected samples were as shown in Tables 2 and 3. According to the data of Table 2, the most chemical compositions of bulk samples were demonstrated averagely as SiO_2, Al_2O_3, CaO, and MgO with mean values 42.82, 9.12, 9.07 and 8.68 %, respectively. The statistical relationship between (CaO+MgO) and L.o.I. shows a more significant correlation (Fig. 3d), indicating the L.o.I. is the crystallization volatile (i.e. H_2O), and it also is a good parameter of alteration with which shows a

positive correlation. You can use that to explain the mean of correlation between the (CaO+MgO) sum and L.o.I. parameter. After XRD results show the major minerals, categorizing as quartz, halite, calcite, and gypsum (Table 4; Fig. 4). Quartz is the main clay mineral in recent sediments and it relates to the climate and weathering pattern of the source area (Rahimpour-Bonab and Abdi 2012). In all topo-soils, the quartz amount showed a mean value of 34%. In this regard, the main quartz mineralogy of the playa averagely was detected based on the ternary plot of Fig. 5, proposed by Von Eynatten et al. (2002).

No.	ID	SiO$_2$	Al$_2$O$_3$	Fe$_2$O$_3$[*]	CaO	Na$_2$O	MgO	K$_2$O	TiO$_2$	MnO	P$_2$O$_5$	Cl$_3$	SO$_4$	L.o.I.

Table (2): Chemical compositions (as wt%) of bulk samples analyzed by XRF method

No.	ID	SiO$_2$	Al$_2$O$_3$	Fe$_2$O$_3$[*]	CaO	Na$_2$O	MgO	K$_2$O	TiO$_2$	MnO	P$_2$O$_5$	Cl$_3$	SO$_4$	L.o.I.
1	207	55.68	10.89	5.77	9.50	1.41	5.33	1.57	0.54	0.10	0.12	0.02	0.01	8.19
2	210	41.88	8.23	5.08	6.29	9.24	9.75	1.66	0.42	0.08	0.10	4.20	3.50	9.56
3	223	40.67	8.16	5.12	7.79	6.70	7.52	1.76	0.43	0.08	0.11	10.50	0.08	10.46
4	233	46.47	9.97	4.98	13.76	1.19	7.29	1.46	0.44	0.08	0.10	0.10	2.80	10.64
5	247	40.52	8.48	5.92	7.90	5.95	8.84	1.92	0.50	0.09	0.12	4.90	4.80	9.31
6	266	41.00	11.69	6.67	12.20	1.86	6.33	2.53	0.59	0.10	0.16	1.01	0.65	14.42
7	277	41.22	9.57	6.72	7.69	6.45	7.97	2.10	0.47	0.10	0.12	5.90	2.60	9.05
8	281	30.55	6.76	5.25	12.06	3.05	10.37	1.26	0.43	0.09	0.13	2.30	10.30	16.77
9	286	43.67	8.82	6.35	7.67	5.82	9.38	1.79	0.49	0.10	0.11	5.30	0.30	9.61
10	290	45.53	9.92	6.57	8.63	4.39	8.53	2.07	0.53	0.11	0.12	3.80	0.06	9.22
11	294	43.65	7.64	7.77	6.95	1.23	15.64	1.52	0.50	0.12	0.11	0.70	1.80	12.10
12	320	43.04	9.37	5.67	8.41	7.34	7.28	1.84	0.45	0.09	0.11	6.90	1.30	8.10

[*]: as total iron , L.o.I.: Loss on Ignition

Table (3): Trace elements data (ppm) of bulk samples analyzed by XRF methods

No.	ID	As	Ba	Ce	Co	Cr	Cu	Nb	Ni	Pb	Rb	Sr	V	Y	Zr	Zn	Mo
1	207	9	355	114	17	258	6	N	137	33	52	595	83	31	173	87	31
2	210	12	212	44	17	333	N	N	357	28	57	212	63	28	85	68	34
3	223	15	257	52	16	110	18	4	190	27	76	403	71	28	126	74	28
4	233	6	370	6	16	390	4	N	273	36	52	501	72	27	146	61	31
5	247	N	282	N	16	107	11	2	204	27	76	965	76	30	158	86	29
6	266	15	419	6	18	111	10	4	177	30	99	524	91	36	164	108	29
7	277	1	309	47	22	154	37	3	339	34	90	476	84	30	137	92	31
8	281	N	272	1	14	178	4	N	251	30	52	1847	73	21	220	67	31
9	286	18	301	58	20	232	19	4	327	35	72	393	80	32	134	87	31
10	290	17	369	N	18	163	17	8	297	35	84	279	79	32	138	102	29
11	294	26	256	20	32	437	9	N	802	40	63	360	80	28	130	100	28
12	320	24	286	52	15	117	50	4	206	33	72	483	74	25	127	78	30

N: Not detected

Table (4): Mineralogy of topo-soil samples by XRD method*

No.	Sample ID	Halite	Quartz	Magnetite	Gypsum	Albite	Calcite	Montmorillonite	Cristobalite	Palygorskite	Muscovite	Dolomite	Hematite
1	207		36			42	21.6	9.8					
2	210	21.8	35				41.9	1.3					
3	223	48.2	28				22.9						
4	233		72	3.4			21.7						5.7
5	247	22	26		27.8			11.2					
6	266		40	1.1		3.4	39		2.1	10.8	3.6		
7	277	18.8	21.5				23.3	6.5	3.5	26.4			
8	281	11.1	43.7		13		26						
9	286	40.8	28							10.1			
10	290	24.6	38.5				26		10.9				
11	294	34	19.8	18.8	14			21					
12	320	29.4	32.2		8.2		28.2						

*: all estimated quantities are approximately
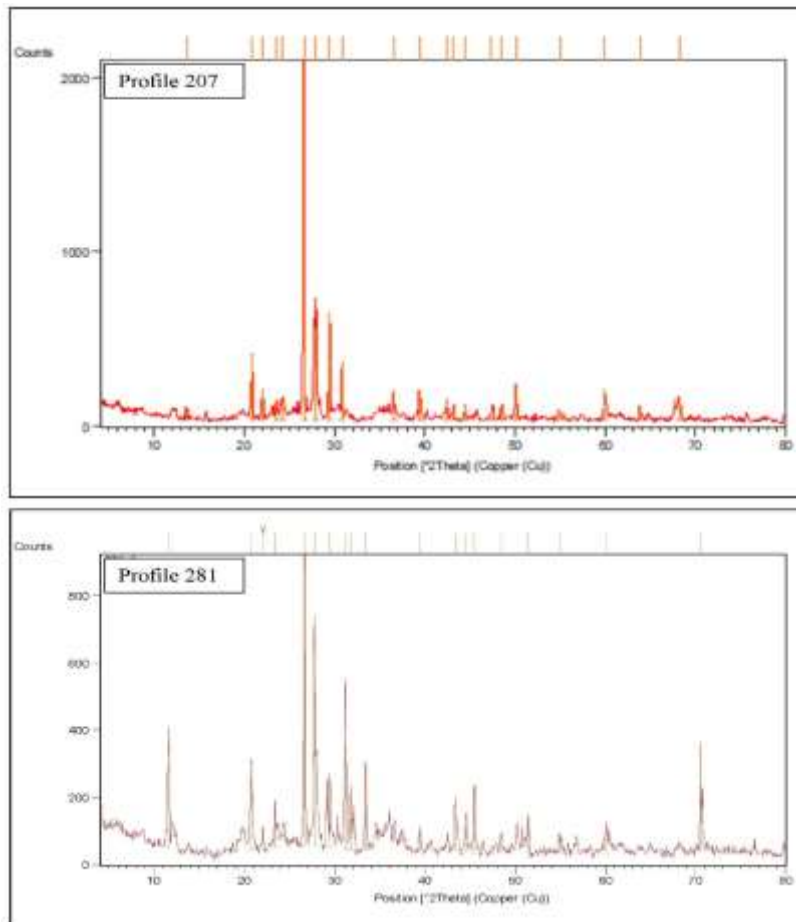
Figure (4): XRD patterns of some topo-soil samples in Sabzevar playa
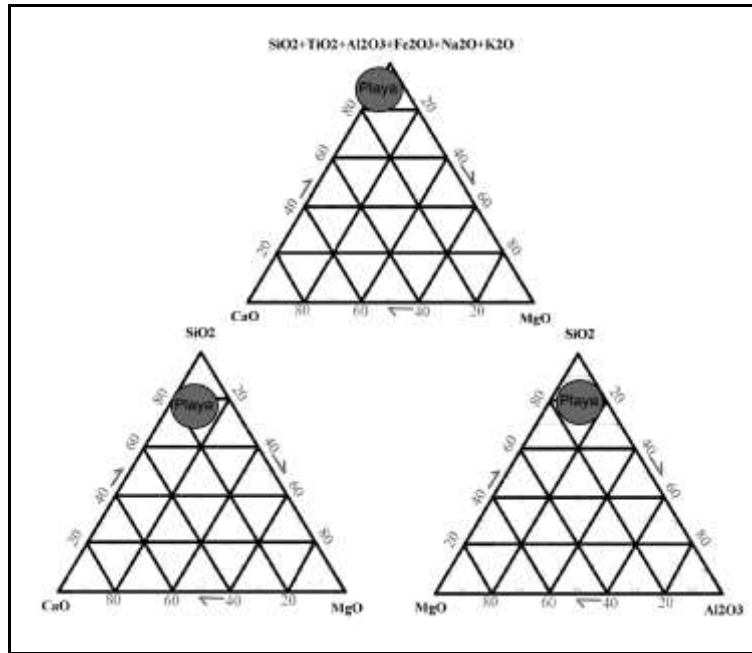
Figure (5): Ternary plots of CaO-MgO-SiO2, MgO-Al2O3-SiO2, and CaO-MgO-other compositions for Sabzevar playa

Afterward, the mean values of halite, calcite, and gypsum have been recorded as 27%, 25%, and 20% in the most topo-soils, indicating a dominant evaporate process. The most calcite amount was observed in topo-soil 210 over the fine-clay ground; however, the most gypsum amount was observed in topo-soil 294 over the salt crusts agreeing on the geomorphologic definition of fieldwork. According to Farpoor et al. (2012), Ca and Mg depositions are observed in central playas of Iran due to the evaporating process of warm climate in the Tertiary period. Nevertheless, high amounts of Si and Al are commonly due to weathering of surrounding formations. The relative concentration of 16 elements was averagely reported in the element enrichment plot (Fig. 6a). In this regard, the element enrichments revealed a higher concentration of clay and heavy minerals.

Based on Smykatz-Kloss, and Roy (2010), the ratio of Na_2O/K_2O can be represented the arid or humid condition of soil units. In Fig. 6b, an interpolation map for the spatial ratio of Na_2O/K_2O was produced. On this basis, the high ratio of the aforementioned unit-less characteristic (>330) is observed in central playa around topo-soils 210 and 223. Also, the negligible ratio of Na_2O/K_2O (<230) is observed in the eastern and western part of the playa for instance around the topo-soils 207 and 290. Hence, the central playa (corresponded to the fine-clay ground) was classified as a very arid soil unit. In the mirror, eastern and western parts of a playa (corresponded to firm-clay ground and salt crusts) are categorized as semi-arid/semi-humid soil units due to groundwater drainage and saline marshland, respectively.
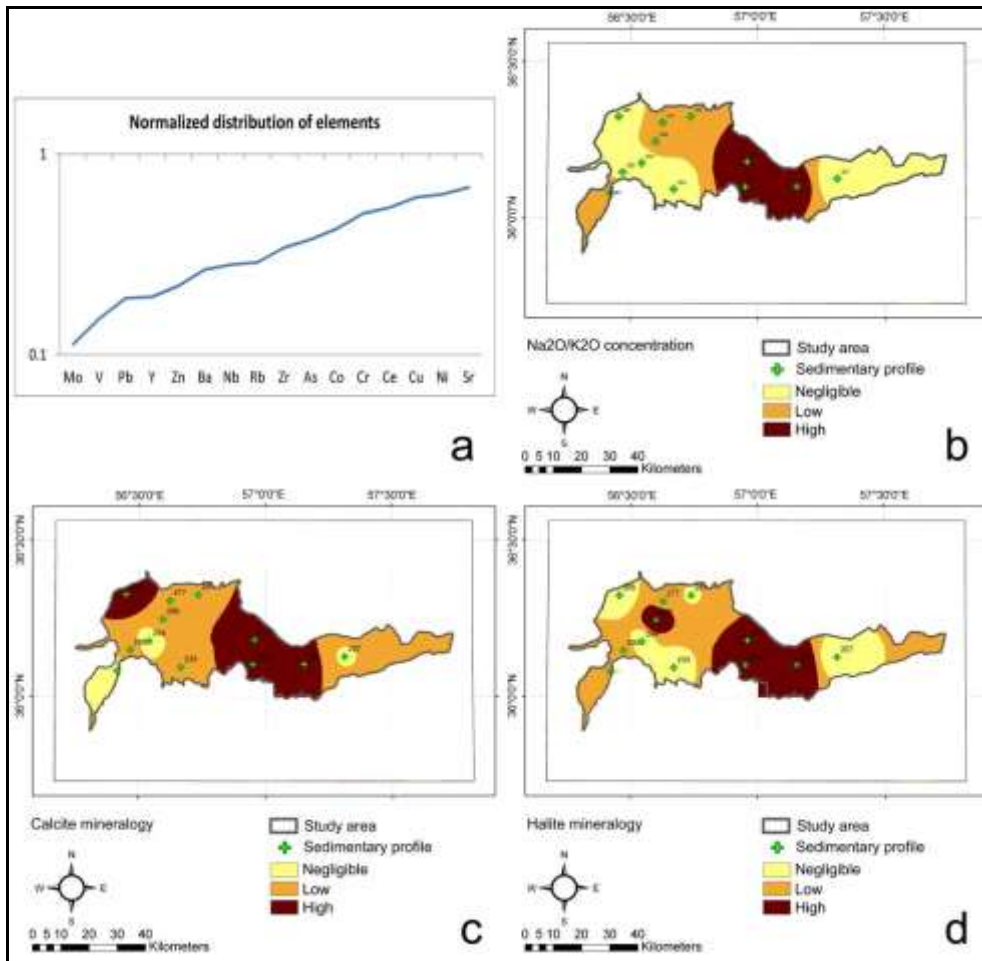
Figure (6): a. Normalized distribution of elemental enrichment plot, b. Geostatistical distribution of of Na2O, K2O ratio, c. Geostatistical distribution of calcite mineralogy, and d. Geostatistical distribution of halite mineralogy

4. Conclusion

All physical-chemical properties of EC, pH, CCE, and soil graining analysis were investigated through selected topo-soils. On this basis, a high concentration of EC (>48 dS/m) is observed in the mid-southern and southern part of playa. The high concentration of CCE (>27 %) is observed in eastern and western playa around topo-soils 207 and 294. Also, a high concentration of pH (>9) is observed in western playa around topo-soils 294. The aforementioned consequence, which gained from the physical-chemical properties of topo-soils, is corresponded to detect of playa's three major geomorphologic landforms in fieldwork observation. Based on graining analysis, some topo-soils represented sandy texture for playa's deposits over the salt crusts and puffy ground indicating osmosis penetration of ground waters

in sediment surface and formation of puffy or salt crust geomorphology. While a silt loam texture was observed over the clay ground indicting firm carbonate surfaces in the study area. Owliaie et al. (2006) and Farpoor et al. (2012) in the playas of Iran have reported a similar mechanism.

According to XRD results, the main minerals of quartz and calcite are observed in the whole playa. The major minerals were categorized as quartz, halite, calcite, and gypsum. Subsequently, the halite, calcite, gypsum indicate evidence of the evaporating process. As well as, it seems a newer deposition pattern of carbonates and chloride in eastern and western parts of the playa, respectively. Nevertheless, central playa shows the ground without alkaline condition and carbonate deposition because marginal wind-

borne deposits and sand dunes have affected it dominantly. On this basis, the major minerals of central playa have been comprised of calcite and halite (Fig. 6c-6d). In these Figures, the negligible concentration of calcite mineralogy (<13%) is observed in western playa around topo-soils 286 and 294. Also, a high concentration of Halite mineralogy (>23%) is observed in the western part of the playa for instance around the topo-soils 294 and 320. The existence of evaporate minerals depends on a cycle of the wet and dried lake during the Holocene. This result confirmed by the occurrence of colder and drier conditions at least between the last glacial maximum (LGM) and the early Holocene in the most playas of Iran especially in central Iran (Krinsley 1970, Hagedorn et al. 1978).

Acknowledgment

Competing interests

The authors declare that they have no competing interests.

Authors' contributions

MP conducted the fieldwork and contributed to the analysis of the data as well as in writing the first draft. AS is a supervisor for the research and MHMG is an adviser. AS and MHMG supervised data analysis and contributed in revising the manuscript and providing the final draft. AS is corresponding the research. All authors read and approved the final manuscript.

References

1. Abrahams AD, Parsons AJ (1994). Geomorphology of Desert Environments, 1st ed. Champan and Hall, London. 674 p.
2. Arche A (2008). Some precisions on the use of the term playa in the geologic literature. Journal of Iberian Geology, 34(1): 5-9.
3. Bagherzadeh A, Mansouri Daneshvar MR (2014). Qualitative Land Suitability Evaluation for Wheat and Barley Crops in Khorasan-Razavi Province, Northeast of Iran. Agric Res, 3(2): 155-164.
4. Briere PR (2000). Playa, Playa-lake, Sabkha: Proposed definitions for old terms. Journal Arid Environments, 45: 1-7.
5. Canton Y, Sole-Benet A, Lazaro R (2003). Soil-geomorphology relations in gypsiferous materials of the Teberans Desert (Almaria, SE Spain). Geoderma, 115: 193-222.
6. Cohen TJ, Jansen JD, Gliganic LA, Larsen JR, Nanson GC, May JH, Jones BG, Price DM, (2015). Hydrological transformation coincided with megafaunalextinction in central Australia. Geology, 43: 195-198.
7. Cooke RU, Warren A (1973) Geomorphology in deserts. University of California Press, Berkeley, pp. 374.
8. Dawson AG (1992). Ice age earth, Late Quaternary Geology and Climate. Routledge, London.
9. DeVogel SB, Magee JW, Manley WF, Miller GH (2004). A GIS-based reconstruction of Late Quaternary paleohydrology: Lake Eyre, arid central Australia. Palaeogeogr. Palaeoclimatol. Palaeoecol, 204: 1-13.
10. Di Piazza A, Conti FL, Noto LV, Viola F, la Loggia G (2011). Comparative analysis of different techniques for spatial interpolation of rainfall data to create a serially complete monthly time series of precipitation for Sicily, Italy. Int. J. Appl. Earth Obs. Geoinf. 13: 396-408.
11. Farpoor MH, Neyestani N, Eghbal MK,

Borujeni IE (2012). Soil-geomorphology relationships in Sirjan playa, south central Iran. Geomorphology, 138: 223-230.

12. Gansser A (1955). New aspects of the geology of Central Iran. Proceedings of the 4th World Petroleum Congress, Rome, Section 1, pp. 280-300.

13. Geological Survey of Iran (2005). Geological sheets of 7262 (Abbas-Abad), 7362 (Davarzan), 7462 (Bashtin), and 7562 (Sabzevar), Scale 1:100,000.

14. Geological Survey of Iran (2016). Digital elevation model data, Scaled at ~10 m pixel size.

15. Glennie KW (1978). Desert sedimentary environments. In: R. W. Fairbridge, J. Bourgeois (eds.), The Encyclopedia of Sedimentology. Dowden, Hutchinson and Ross, Stroudsburg, 247-251.

16. Gholami H, Kordestani MD, Li J, Telfer MW, Fathabadi A (2019). Diverse sources of aeolian sediment revealed in an arid landscape in southeastern Iran using a modified Bayesian un-mixing model. Aeolian Res. 41: 100547.

17. Hagedorn H, Haars W, Busche D, Grunert J (1978). Some geomorphological observations from the Shir Kuh Mountains area. Geography: Journal of the Association of Iranian Geographers 1: 10-15.

18. Handford CR (1981). A Process-Sedimentary Framework for Characterizing Recent and Ancient Sabkhas: Sedimentary, Geology, 30: 255-265.

19. Harrison SP (1993). Late Quaternary lake-level changes and climates of Australia. Quat. Sci. Rev., 12: 211-231.

20. Hijmans RJ, Cameron SE, Parra JL, Jones PG, Jarvis A (2005). Very High Resolution Interpolated Climate Surfaces for Global Land Areas. International Journal of Climatology, 25(15):1965-1978

21. Kearey P (2009). The Encyclopedia of the Solid Earth Sciences. John Wiley & Sons, pp 736.

22. Kramar U (1997). Advances in energy-dispersive X-ray fluorescence. Journal of Geochemical Exploration, 58: 73-80.

23. Krinsley DB (1970). A geomorphological and paleoclimatological study of the playas of Iran. Geological survey of United States Department of Interior, Washington DC, pp 320.

24. Lamas F, Irigaray C, Oteo C, Chacon J (2005). Carbonate content for engineering purposes with particular regard to marls. Eng Geol., 81:32-41.

25. Lancaster N, Wolfe S, Thomas D, Bristow C, Bubenzer O, Burrough S, Duller G, Halfen A, Hesse P, Roskin J, Singhvi A, Tsoar H, Tripaldi A, Yang X, Zarate M (2016). The INQUA Dunes Atlas chronologic database. Quat. Int. 410: 3-10.

26. Leighton CL, Thomas SG, Bailey RM (2014). Reproducibility and utility of dune luminescence chronologies. Earth-Sci. Rev. 129: 24-39.

27. Leon JX, Cohen TJ (2012). An improved bathymetric model for the modern and palaeo Lake Eyre. Geomorphology, 173-174: 69-79.

28. Li H, Yang X (2015). Spatial and temporal patterns of aeolian activities in the desert belt of northern China revealed by dune chronologies. Quat. Int. 410: 58-68.

29. Magee JW, Miller GH, Spooner NA, Questiaux D (2004). Continuous 150 k.y. monsoon record from Lake Eyre, Australia: insolation-forcing implications and unexpected Holocene failure. Geology, 32: 885-888.

30. May JH, Barrett A, Cohen TJ, Jones BG, Price D, Gliganic LA (2015). Late Quaternary evolution of a playa margin at Lake Frome, South Australia. Journal of Arid Environments, 122: 93-108.

31. Moussavi-Harami R, Mahboubi A, Khanehbad M (2004). Analysis of controls on downstream fining along three gravel-bedrivers in the Band-e-Golestan drainage

basin NE Iran. Geomorphology 61: 143-153.

32. Nikolopoulos EI, Borga M, Creutin JD, Marra, F. (2015). Estimation of debris flow triggering rainfall: Influence of rain gauge density and interpolation methods. Geomorphology 243: 40-50.

33. Owliaie HR, Abtahi A, Heck RJ (2006). Pedogenesis and clay mineralogical investigation of soils formed on gypsiferous and calcareous materials on a transect, Southwestern Iran. Geoderma 134: 62-81.

34. Rahimpour-Bonab H, Abdi L (2012). Sedimentology and origin of Meyghan lake/playa deposits in Sanandaj-Sirjan zone, Iran. Carbonates Evaporites, 27: 375-393.

35. Razmi R, Balyani S, Mansouri Daneshvar MR (2017). Geo-statistical modeling of mean annual rainfall over the Iran using ECMWF database. Spatial Information Research 25: 219-227.

36. Rosen MR (1994). The importance of groundwater in playas. A review of playa classifications and the sedimentology and hydrology of playa. Geol Soc Am Special Paper, 289: 1-18.

37. Roy PD, Smykatz-Kloss W, Sinha R (2006). Late Holocene geochemical history inferred from Sambhar and Didwana playa sediments, Thar Desert, India: Comparison and synthesis. Quaternary International, 144: 84-98.

38. Sinha R, Smykatz-Kloss W, Stüben D, Harrison SP, Berner Z, Kramar U (2006). Late Quaternary palaeoclimatic reconstruction from the lacustrine sediments of the Sambhar playa core, Thar Desert margin, India. Palaeogeography, Palaeoclimatology, Palaeoecology, 233: 252-270.

39. Smykatz-Kloss W, Roy PD (2010). Evaporite mineralogy and major element geochemistry as tools for palaeoclimatic investigations in arid regions: A synthesis. Boletín de la Sociedad Geológica Mexicana 62(3): 379-390.

40. Statistical Centre of Iran (2016). Macro results of statistical survey. http://www.amar.org.ir. Accessed 2016.

41. Street-Perrott F, Harrison S (1985). Lake levels and Climate Reconstruction. Paleoclimate Analysis and Modeling, pp. 291-340.

42. Thomas SG (1997). Reconstructing ancient arid environments. In: Thomas SG (Ed.), Arid Zone Geomorphology. Wiley, London, pp. 577-607.

43. Thomas SG, Burrough SL (2013). Luminescence-based dune chronologies in southern Africa: Analysis and interpretation of dune database records across the subcontinent. Quat. Int. 410(29): 30-45.

44. US Salinity Laboratory Staff (1954). Diagnosis and improvement of saline and alkali soils. US Department of Agriculture Handbook 60, Washington, DC.

45. Vaezi A, Ghazban F, Tavakoli V, Routh J, Beni AN, Bianchi TS, Curtis JH, Kylin H (2019). A Late Pleistocene-Holocene multi-proxy record of climate variability in the Jazmurian playa, southeastern Iran. Palaeogeogr. Palaeoclimatol. Palaeoecol. 514(15): 754-767.

46. Wang Q, Ni J, Tenhunen J (2005). Application of a geographically weighted regression analysis to estimate net primary production of chinese forest ecosystem. Global Ecology and Biogeography 14: 379-393.

47. Yang L, Dong Y, Huang D (2018). Morphological response of coastal dunes to a group of three typhoons on Pingtan Island, China. Aeolian Res. 32: 210-217.

48. Watson A (1983). Evaporite sedimentation in non-marine environments. In: Goudie AS, Pye K (eds.), Chemical sediments and geomorphology: precipitates and residua in the near-surfaceenvironment. Academic Press, London, pp. 163-185.